




OPEN

Discriminators of pseudoprogression and true progression in high-grade gliomas: A systematic review and meta-analysis

Chris Taylor¹, Justyna O. Ekert², Viktoria Sefcikova¹, Naomi Fersht³ & George Samandouras^{2,4}

High-grade gliomas remain the most common primary brain tumour with limited treatments options and early recurrence rates following adjuvant treatments. However, differentiating true tumour progression (TTP) from treatment-related effects or pseudoprogression (PsP), may critically influence subsequent management options. Structural MRI is routinely employed to evaluate treatment responses, but misdiagnosis of TTP or PsP may lead to continuation of ineffective or premature cessation of effective treatments, respectively. A systematic review and meta-analysis were conducted in accordance with the Preferred Reporting Items for Systematic Reviews and Meta-analyses method. Embase, MEDLINE, Web of Science and Google Scholar were searched for methods applied to differentiate PsP and TTP, and studies were selected using pre-specified eligibility criteria. The sensitivity and specificity of included studies were summarised. Three of the identified methods were compared in a separate subgroup meta-analysis. Thirty studies assessing seven distinct neuroimaging methods in 1372 patients were included in the systematic review. The highest performing methods in the subgroup analysis were DWI (AUC = 0.93 [0.91–0.95]) and DSC-MRI (AUC = 0.93 [0.90–0.95]), compared to DCE-MRI (AUC = 0.90 [0.87–0.93]). 18F-fluoroethyltyrosine PET (18F-FET PET) and amide proton transfer-weighted MRI (APT_w-MRI) also showed high diagnostic accuracy, but results were based on few low-powered studies. Both DWI and DSC-MRI performed with high sensitivity and specificity for differentiating PsP from TTP. Considering the technical parameters and feasibility of each identified method, the authors suggested that, at present, DSC-MRI technique holds the most clinical potential.

High-grade gliomas (HGGs) remain some of the most common subtypes of primary brain tumours¹ with standard treatment options including surgical debulking followed by radiotherapy, and adjuvant or concurrent chemoradiation therapy (CCRT) with temozolomide, in world health organisation (WHO) grade III and IV, respectively^{2,3}. However, HGGs are characterised with early and high recurrence rates⁴. Routine MRI scans are often reported to display tumour volume growth, new or enlarged areas of contrast enhancement, or oedema which may represent either TTP or treatment effects called PsP. The latter can be transient and is often clinically asymptomatic⁵, but is often misdiagnosed as TTP, leading to premature cessation of potentially effective treatments and often substitution for less effective, second-line treatments⁶. Conversely, TTP misdiagnosed as PsP can complicate the monitoring of tumour progression by increasing waiting times, negatively influencing treatment outcomes⁷.

A meta-analysis by Abbasi and colleagues⁸ found a form of pseudoprogression in 36% of 2603 patients harbouring HGGs. However, lack of standardised definitions for PsP and accurate diagnostic methods resulted

¹UCL Queen Square Institute of Neurology, University College London, Gower St., Bloomsbury, Queen Square, London WC1E 6BT, UK. ²Wellcome Centre for Human Neuroimaging, University College London, 12 Queen Square, London, UK. ³Department of Oncology, University College London Hospitals NHS Foundation Trust, London, UK. ⁴Victor Horsley Department of Neurosurgery, The National Hospital for Neurology and Neurosurgery, Queen Square, London, UK. ✉email: skgtayl@ucl.ac.uk

in varying prevalence estimates in the literature. PsP occurs within the first 3 months following radiotherapy almost 60% of the time, with a range that is usually between 2 and 6 months^{9,10}. It is physiologically and clinically comparable to radiation necrosis, which generally occurs 3–12 months after therapy¹¹. It is postulated that radiotherapy induces local endothelial cell death, leading to increased vascular permeability, perilesional oedema, and mass effect¹². This gives a localised area of contrast enhancement on structural MRI that requires further assessment to distinguish from TTP¹². Interestingly, patients with confirmed PsP generally have an improved prognosis¹³, although this may be subject to survivor bias due to the usually longer time PsP requires to manifest⁵.

Standard practice currently involves clinical confirmation of PsP using serial MRI, histopathology via invasive brain biopsy, and/or application of the RANO criteria¹⁴. This practice is time-consuming and can be subjective, and histological confirmation requires admission and additional surgery under general anaesthetic. Watchful surveillance can further delay clinical decision making, significantly affecting prognosis⁷. Several imaging methods allowing early differentiation between PsP and TTP, are currently under investigation and demonstrate high sensitivity and specificity compared to histological confirmation.

Current work has applied dynamic susceptibility contrast perfusion MRI (DSC-MRI), dynamic contrast-enhanced perfusion MRI (DCE-MRI), diffusion-weighted MRI (DWI), arterial spin labelling (ASL), amide proton transfer-weighted MRI (APT_w-MRI), 18F-fluoroethyltyrosine PET (FET-PET), and combinations of these modalities. All considered modalities have shown a degree of diagnostic value, but their relative clinical potential is still not well established. The aim of this systematic review and meta-analysis is to provide a comprehensive comparison of PsP and TTP differentiators based on measures of sensitivity, specificity, and clinical applicability. The advent of novel, more quantitative methods of diagnosis are also discussed.

Methods

Inclusion/exclusion criteria. *Study design.* Randomised controlled trials, controlled clinical trials, and prospective or retrospective observational studies were included with a sample size threshold $n \geq 10$. Conference abstracts, grey literature, and articles with no available English translation were excluded at the screening stage.

Population. Studies included adult patients (≥ 16 years old) receiving radiotherapy or chemoradiotherapy following a diagnosis of a high-grade glioma. Studies needed to specify the proportion of the sample that exhibited PsP, which was confirmed no more than 6 months following radiotherapy.

Intervention. Studies assessed the diagnostic accuracy of a method used to differentiate TTP from PsP in HGG patients.

Outcome. Study outcomes reported a method's diagnostic sensitivity and specificity compared to the gold standard of expert assessment, and/or according to the RANO criteria.

Search strategy. The search strategy was devised in line with the recommendations in Bramer and colleagues¹⁵. The entirety of Embase, MEDLINE, and Web of Science were searched on the 20th of May 2022. The first 200 results of a Google Scholar search were also included. The full search strategy is detailed in Supplementary Material A. Studies returned by the search were compiled and screened for data extraction in accordance with the Preferred Reporting Items for Systematic Reviews and Meta-Analysis (PRISMA) method¹⁶. All titles and selected abstracts were screened on the basis of the inclusion criteria, and full texts were subsequently reviewed. The full selection process is shown in Fig. 1, and the full exclusion criteria listed in Supplementary Material C. The protocol was registered to PROSPERO prior to searching (ID CRD42022218217).

Data extraction and quality assessment. Data were extracted onto a spreadsheet with the following variables: (1) first author and year of publication; (2) neuroimaging method of discrimination between TTP and PsP; (3) sample size and demographics, including proportion of patients that presented with PsP; (4) administration of radiotherapy / chemoradiation therapy / CCRT; (5) tumour grade; and (6) sensitivity and specificity measures. Extracted data were inputted into Cochrane Review Manager 5.4¹⁷. The review was conducted according to the Meta-analysis of Observational Studies in Epidemiology (MOOSE) proposal¹⁸. The quality of included studies and risk of bias was assessed with the Quality Assessment of Diagnostic Accuracy (QUADAS-2) tool by two independent and blinded reviewers C.T. and V.S.¹⁹. Any disagreement was resolved with consensus.

In the included studies, sensitivity was defined as the proportion of patients with histopathologically confirmed TTP that presented as such with the modality of choice, or the true positive rate. Specificity was defined as the proportion of patients with histopathologically confirmed PsP that presented as such, or the true negative rate. A high sensitivity and specificity constitute a high diagnostic accuracy, which in turn represents the overall precision of clinical decisions. Studies that did not meet this definition of sensitivity and specificity were excluded during data extraction.

Data synthesis and statistical analysis. All included studies were presented in a forest plot. A separate subgroup meta-analysis was performed to compare the three most prevalent methods among studies: DSC-MRI ($n = 12$), DCE-MRI ($n = 4$), and DWI ($n = 12$). For the systematic review, the primary outcomes were TTP and PsP discrimination method sensitivity and specificity. For the subgroup meta-analysis, the primary outcomes were pooled sensitivity, specificity, and area under the summary receiver operating characteristics curve (SROC AUC)²⁰.

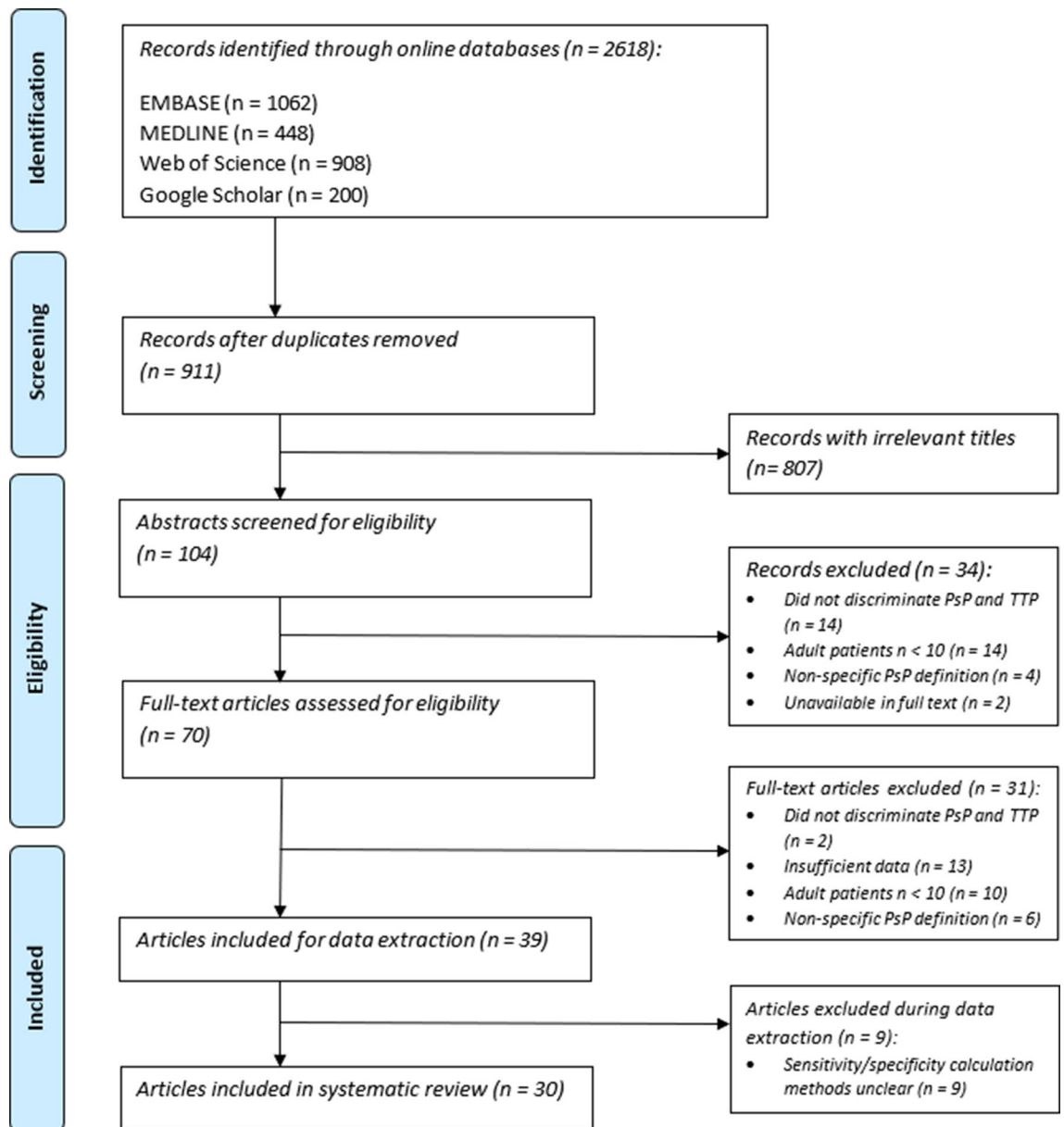


Figure 1. PRISMA flow chart of the study selection process. sP = pseudoprogression; TTP = true tumour progression.

Within-group heterogeneity was assessed using the I^2 variable, which describes the proportion of variation in study results that can be attributed to heterogeneity²¹. To account for the high heterogeneity of data across multiple modalities, data inputted into Cochrane Review Manager 5.4 were analysed using a random effects model, which assumes individual effects are uncorrelated with independent variables. Pooled sensitivity, specificity, likelihood ratio, negative likelihood ratio, diagnostic odds ratio (DOR) and SROC AUC were calculated using the MIDAS (meta-analytical integration of diagnostic test accuracy studies) package in STATA²². Forest plots and a subgroup analysis SROC plot were generated in Cochrane Review Manager 5.4. For studies reporting median instead of mean age, the mean was estimated according to previously established methods²³.

Consent to participate. Informed consent was obtained from all individual participants included in the study.

Results

Search results. Following deduplication, the literature search yielded 911 abstracts. Following abstract screening, 70 full-text articles were retrieved and assessed for eligibility. Data was extracted from 39 articles, 9 of which did not report sufficient information to allow for calculation of sensitivity and specificity values, and therefore were excluded. A total of 30 studies totalling 1372 patients were included in the systematic review (see Table 1).

Method	Study	Sample size	PsP/TTP	M/F	Mean age (yrs)	WHO grade	Radiation therapy
DSC-MRI	Baek et al. ⁶³	79	37/42	46/33	51	IV	CRT-TMZ
	Cha et al. ⁶⁴	35	24/11	18/17	49	IV	CRT-TMZ
	Kerkhof et al. ³⁴	58	26/32	41/17	60	IV	CRT-TMZ
	Kong et al. ⁶⁵	59	26/33	49/10	50	IV	CRT-TMZ
	Mangla et al. ⁶⁶	19	7/12	NS	63	IV	RT-TMZ
	Martínez-Martínez et al. ³⁷	34	17/17	14/20	48	III-IV	CRT-TMZ
	Mihailović et al. ⁶⁷	40	8/32	37/3	51	IV	RT-TMZ
DSC-MRI, DWI	Kim et al. ²⁴	34	20/14	25/9	62	IV	CRT-TMZ
	Prager et al. ²⁵	51	8/43	NS	55	IV	CRT-TMZ
DSC-MRI, ASL	Jovanovic et al. 2017 ²⁷	31	11/20	21/10	49	IV	RT-TMZ
DSC-MRI & ASL	Choi et al. ²⁸	62	28/34	37/25	49	IV	CRT-TMZ
DSC-MRI & DCE-MRI	Elshafeey et al. ²⁹	98	22/76	57/41	50	IV	CRT-TMZ
DSC-MRI, DWI, DSC-MRI & DWI	Shi et al. ²⁶	34	12/22	24/10	47	III-IV	CRT-TMZ
DWI	Bulik et al. ⁶⁸	24	6/18	17/7	50	IV	CRT-TMZ
	Chu et al. ⁶⁹	30	15/15	16/14	51	IV	CRT-TMZ
	Kazda et al. 2016 ⁷⁰	39	10/29	28/11	51	IV	CRT-TMZ
	Lee et al. ⁷¹	22	12/10	NS	49	IV	CRT-TMZ
	Patel et al. ⁷²	76	30/46	46/30	56	IV	CRT-TMZ
	Reimer et al. ⁷³	35	7/28	26/9	58	III-IV	CRT-TMZ
	Song et al. ⁷⁴	20	10/10	10/10	51	IV	CRT-TMZ
	Wu et al. ⁷⁵	40	16/24	28/12	46	III/IV	CRT-TMZ
	Yoo et al. ⁷⁶	42	18/24	27/15	61	IV	CRT-TMZ
DCE-MRI	Nam et al. ⁷⁷	37	22/15	26/11	58	IV	CRT-TMZ
	Suh et al. ⁷⁸	79	37/42	36/43	49	IV	CRT
	Thomas et al. ⁷⁹	37	13/24	25/12	63	IV	CRT-TMZ
	Yun et al. ⁸⁰	33	16/17	22/11	55	IV	CRT-TMZ
18F-FET PET	Galldiks et al. ³⁰	22	11/11	14/8	56	IV	CRT-TMZ
APTw-MRI	Ma et al. ³¹	32	12/20	21/11	56	III-IV	CRT-TMZ
Conventional MRI*	Sun et al. ⁸¹	77	26/51	40/37	49	IV	CCRT-TMZ
	Young et al. ³²	93	30/63	58/35	59	IV	CRT-TMZ

Table 1. Details of included studies. APTw-MRI = amide proton transfer-weighted MRI; ASL = arterial spin labelling; CRT-TMZ = chemoradiotherapy with adjuvant temozolomide; NS = not specified, TTP = true progression. Conventional MRI included contrast-enhanced T1-weighted and T2-weighted acquisitions.

Of the 1372 patients, 538 (39.2%) cases were confirmed to have PsP following radiotherapy, according to histological examination and/or examination according to the RANO criteria. The mean age across the studies was 54, with a range of study mean age of 46 to 62 years. Based on 27 studies with relevant reporting, the male/female ratio was 1.4/1.

Seven distinct methods for differentiating PsP from TTP were identified: DSC-MRI, DWI, DCE-MRI, ASL, APTw-MRI, 18F-FET PET, and conventional MRI. Three studies compared DSC-MRI and DWI²⁴⁻²⁶ and one compared DSC-MRI and ASL²⁷. Combinations of modalities applied included DSC-MRI & ASL, DSC-MRI & DCE-MRI, and DSC-MRI & DWI^{26,28,29}.

All methods were summarised in the non-subgroup analysis (Fig. 2). Three studies reported 100% sensitivity and specificity: two using DSC-MRI, and one using DWI. FET-PET reported high overall sensitivity and specificity in the included study³⁰. The included paper that applied APTw-MRI also reported a high diagnostic accuracy (sensitivity = 95%, specificity = 0.92%)³¹. These modalities had insufficient data to be included in the subgroup analysis.

The lowest sensitivity (38%) for identifying tumour progression was reported by Young and colleagues³², who examined visual signs such as enhancement on conventional MRI across 93 patients. The only other paper that applied conventional MRI acquisitions used a radiomics-based approach, but still reported relatively low diagnostic accuracy³³. The lowest specificity for true progression (23%) was reported by Kerkhof and colleagues³⁴, which differentiated PsP and TTP by using visual interpretation of relative cerebral blood volume (rCBV) maps from DSC-MRI. Sensitivity tended to be higher than specificity in the majority of included studies.

Subgroup analysis. Three distinct methods across 25 studies reported sufficient data to include in a separate set of subgroup analyses: DSC-MRI (n = 12), DCE-MRI (n = 4), and DWI (n = 12). Subgroups included

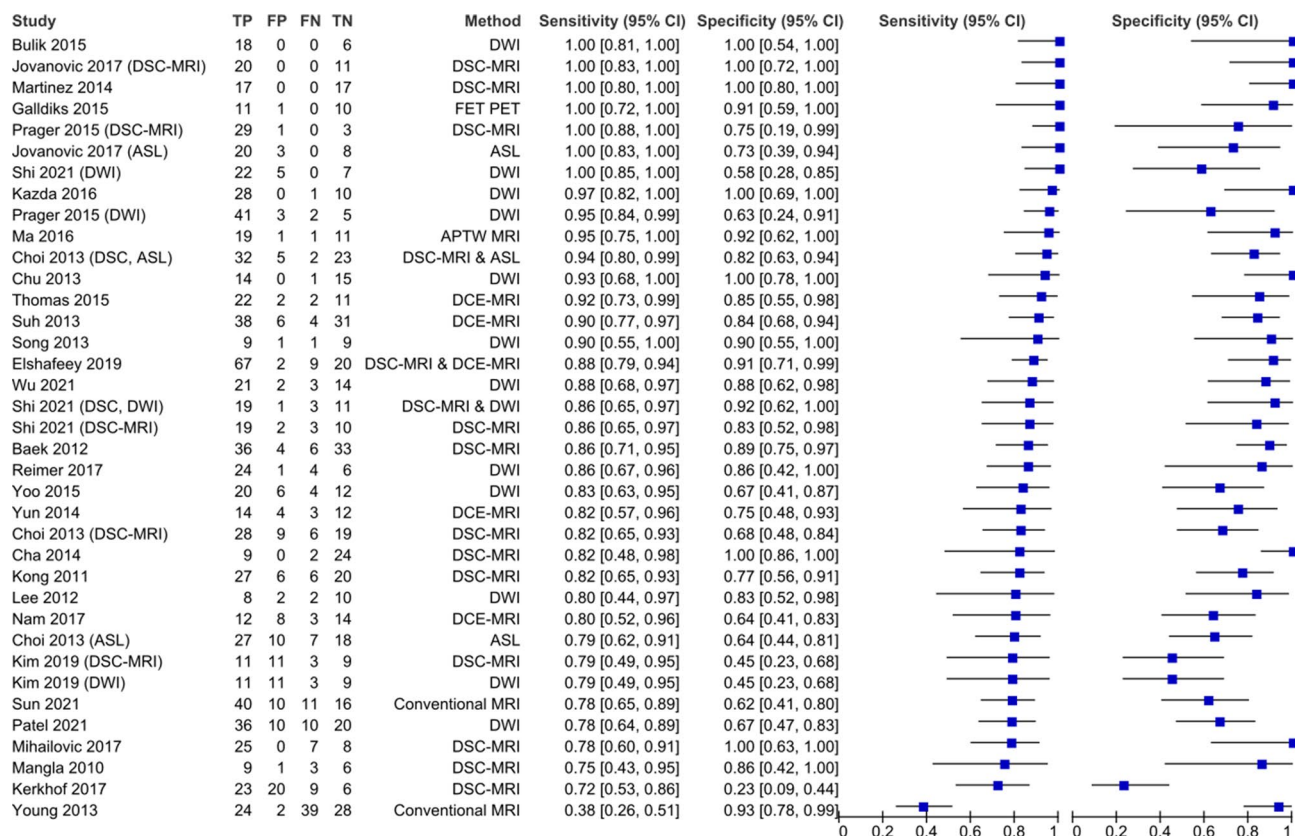


Figure 2. Forest plot assessing various methods of differentiation of pseudoprogression from true progression according to measures of sensitivity and specificity. APTw-MRI = amide proton transfer-weighted MRI; ASL = arterial spin labelling; DCE-pMRI = dynamic contrast-enhanced perfusion MRI; DSC-pMRI = dynamic susceptibility contrast perfusion MRI; DWI = diffusion weighted imaging; FET PET = [¹⁸F]fluoroethyltyrosine PET.

518, 186, and 459 patients, respectively. Studies by Kim and colleagues²⁴, Prager and colleagues²⁵, and Shi and colleagues²⁶, measured DSC-MRI and DWI separately and thus appear twice in the subgroup forest plot (Fig. 3).

All three subgroups had a high diagnostic accuracy for differentiating PsP from TTP (Figs. 3, 4) supported by high diagnostic odds ratios (Table 2). DWI demonstrated the highest average sensitivity (0.90 [0.84–0.94]), while DSC-MRI demonstrated the highest average specificity (0.88 [0.70–0.96]). A high overall diagnostic accuracy was however demonstrated by all subgroups: DSC-MRI (SROC AUC = 0.93 [0.90–0.95], DOR = 57 [12–268]), DCE-MRI (SROC AUC = 0.90 [0.87–0.93], DOR = 24 [9–60]), and DWI (SROC AUC = 0.93 [0.91–0.95], DOR = 42 [12–268]).

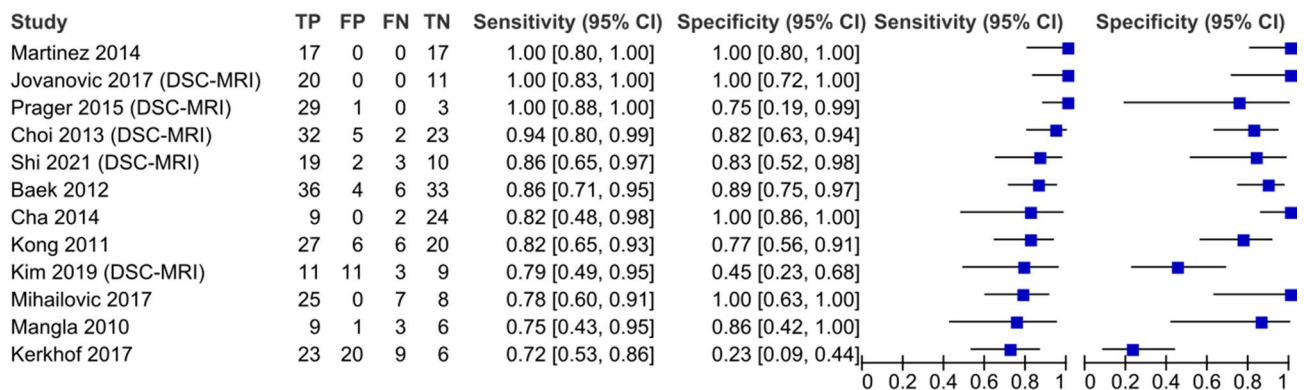
Heterogeneity for both DCE-MRI and DWI was calculated as $I^2 = 0\%$, but high heterogeneity was reported in the DSC-MRI subgroup ($I^2 = 79\%$). This heterogeneity was more predominant in the reported specificity ($I^2 = 85\%$). The DSC-MRI subgroup had the greatest amount of variation in methodology. However, true heterogeneity is unlikely to be zero in the DCE-MRI and DWI subgroups, and the small sample size may have led to an underestimation³⁵.

Quality assessment. Thirteen of the included 30 studies were determined to have a high risk of bias. Nearly all included studies had a high risk of bias in the index test section. The parameter cut-off values were not pre-specified and instead defined post-hoc. High risk of bias was also apparent in the patient selection category. This was largely due to inclusion of patients who received steroids with standard chemoradiotherapy in some studies. Details of patient enrolment and inclusion/exclusion were also unclear in some studies, and nearly 40% of total included patients presented with PsP, which is higher than previous estimates⁸. There were low applicability concerns observed in the included studies. The full risk of bias table and a more detailed summary of quality assessment across all studies is detailed in Supplementary Material B1 & B2.

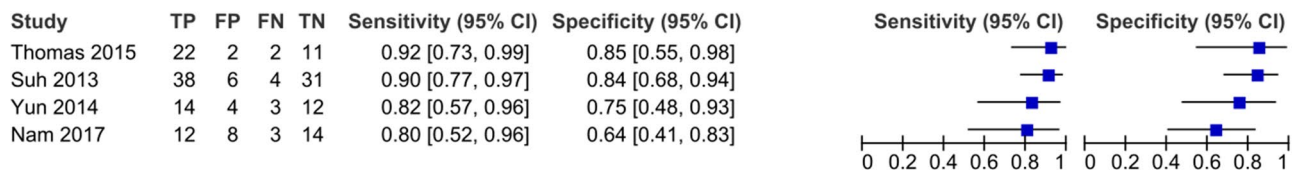
Discussion

The current systematic review and meta-analysis aimed to compare the most promising methods of the differentiation of PsP and TTP in patients with high-grade gliomas. A prior meta-analysis has compared the utility of DWI and PWI (perfusion-weighted imaging) for discriminating PsP and TTP³⁶. Consistent with our results, they found the two modalities to be very comparable in terms of diagnostic accuracy. In contrast to the study by

DSC-MRI



DCE-MRI



DWI

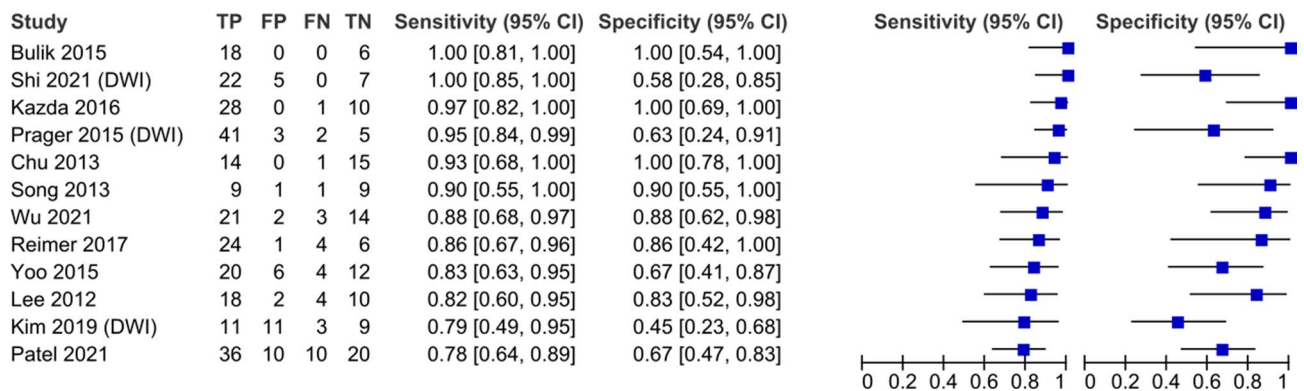


Figure 3. Forest plot subgroup analysis assessing the diagnostic ability of DSC-MRI, DCE-MRI, and DWI. See Fig. 2 for list of abbreviations.

Tsakiris and colleagues, our inclusion criteria were not limited to two methods only. Furthermore, we consider each modality in the context of its clinical utility, aiming to provide a recommendation for physicians.

A total of seven PsP and TTP imaging discriminators have been identified in the literature: (1) DSC-MRI, (2) DWI, (3) DCE-MRI, (4) ASL, (5) APTw-MRI, (6) 18F-FET PET, and (7) conventional MRI acquisitions. Three combinations of the methods were identified: (1) DSC-MRI & DCE-MRI, (2) DSC-MRI & DWI, and (3) DSC-MRI & ASL.

The results reported in the current meta-analysis were generally very positive. This may be attributed to a publication bias in which positive results are favoured. Strong positive results on methods for which little data on diagnostic accuracy is available, should be interpreted with caution.

Diffusion and perfusion-based methods. Our meta-analysis found that DWI, DSC-MRI and DCE-MRI have high potential for differentiating PsP and TTP in patients harbouring HGGs. DSC-MRI and DWI may have some advantage over DCE-MRI, but due to inter-study variations no statistical conclusions can be made. Out of these three methods, DWI demonstrated the highest sensitivity for detecting TTP (0.90 [0.84–0.94]), and DSC-MRI demonstrated the highest specificity (0.88 [0.70–0.96]). Overall accuracy results based on SROC AUC scores were indistinguishable between DWI and DSC-MRI.

Assessment of imaging results using pre-specified parameter cut-off values was associated with higher sensitivity and specificity values in comparison to studies that relied on visual inspection. Kerkhof and colleagues³⁴ visually inspected rCBV colour maps to differentiate PsP from TTP, which yielded 72% sensitivity and 23% specificity, both of which were the lowest of the twelve studies included in the DSC-MRI subgroup, which may have negatively skewed averaged results. In contrast, two other included DSC-MRI studies^{31,37} reported 100% sensitivity and 100% specificity using parameter cut-off values to differentiate PsP from TTP. Jovanovic

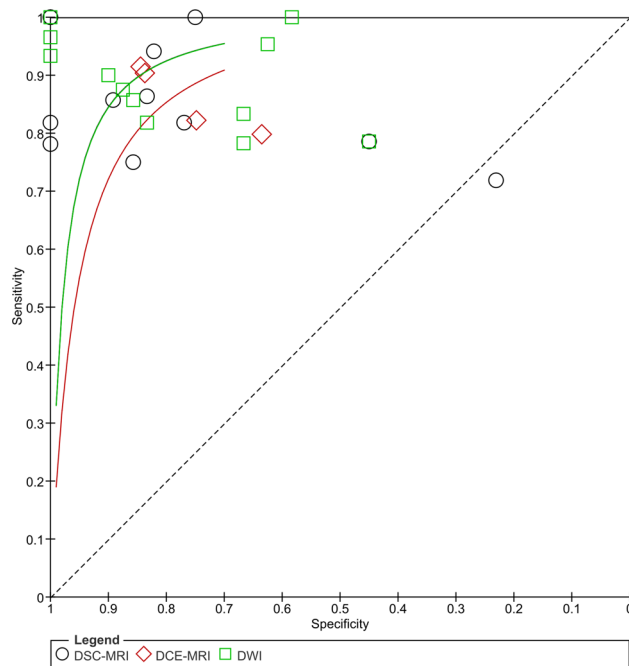


Figure 4. Summary receiver operating characteristics plot comparing diagnostic ability of subgrouped modalities. DSC-MRI, DCE-MRI and DWI are included in the SROC plot and compared according to the mean reported sensitivity and specificity of the studies in the subgroup.

	Pooled		Likelihood ratio		DOR	SROC AUC
	Sensitivity	Specificity	Positive	Negative		
DSC-MRI	0.88 [0.81–0.93]	0.88 [0.70–0.96]	7.6 [2.6–22.1]	0.13 [0.07–0.24]	57 [12–268]	0.93 [0.90–0.95]
DCE-MRI	0.88 [0.79–0.93]	0.77 [0.66–0.86]	3.8 [2.4–6.1]	0.16 [0.09–0.29]	24 [9–60]	0.90 [0.87–0.93]
DWI	0.90 [0.84–0.94]	0.82 [0.68–0.91]	5.0 [2.6–9.6]	0.12 [0.07–0.21]	42 [14–126]	0.93 [0.91–0.95]

Table 2. Summary statistics comparing DSC-MRI, DCE-MRI, and DWI. DOR = diagnostic odds ratio; LR = likelihood ratio; SROC AUC = Summary receiver operator characteristics area under curve.

and colleagues used a ratio of 2.89 of normalized CBV between the lesion and normal-appearing tissue, while Martínez-Martínez and colleagues used an rCBV value of 0.9.

Direct comparisons between the diagnostic accuracies of DSC-MRI and DWI were provided in studies by Kim and colleagues²⁴, Prager and colleagues²⁵, and Shi and colleagues²⁶. Kim and colleagues found that the maximum CBV parameter of DSC-MRI and the mean apparent diffusion coefficient (ADC) of DWI differentiated PsP and TTP with the same sensitivity (79%) and specificity (45%) in 34 patients²⁴. In the other two studies, DSC-MRI outperformed DWI in specificity, but both reported similarly high sensitivity results^{25,26}.

Choi and colleagues²⁸ investigated the diagnostic accuracy of DSC-MRI and ASL. The sensitivity and specificity of DSC-MRI were determined as 82.4% and 67.9%, respectively and 79.4% and 64.3%, respectively, for ASL. A combination of the two modalities resulted in an increased sensitivity and specificity of 94.1% and 82.1%, although this did not represent a significant increase in diagnostic accuracy ($p = 0.133$). Jovanovic and colleagues²⁷ separately assessed DSC-MRI and ASL, and quantitative analysis found both methods to yield 100% sensitivity in their patient sample. For specificity, ASL scored 73% compared to 100% for DSC-MRI. All four included diffusion/perfusion-based methods show clinical potential. DSC-MRI is currently the most widely employed, and its protocol and acquisition parameters are already well-defined³⁸.

FET PET. There has been increasing interest in the application of PET in differentiating between PsP and TTP. One study included in this review used 18F-FET PET and found the maximal tumour-to-brain ratio (TBR_{max}) differentiates between the two with 100% specificity and 91% sensitivity at a cut-off of 2.3, in a sample of 22 patients³⁰. A similar cut-off value of $TBR_{max} = 2.55$ was reported by Kebir and colleagues³⁹. In the same study, a linear discriminant analysis-based algorithm was trained on IDH-wildtype glioblastoma FET PET features and compared the results to a conventional FET PET analysis. The algorithm provided an AUC of 0.93, which was higher than the AUC for TBR_{max} of 0.68.

Several other FET PET studies in the literature were found during the search but did not meet the inclusion criteria, since patients were scanned more than 6 months following diagnosis. This may be a contributing factor

	Dynamic susceptibility contrast (DSC)	Diffusion-weighted imaging (DWI)	Dynamic contrast enhanced (DCE)	Arterial spin labelling (ASL)	Amide proton transfer-weighted (APT _w)	18F-FET PET
Sensitivity/specificity*	0.88 / 0.88	0.90 / 0.82	0.88 / 0.77	-	-	-
Use of contrast agent/ radioactive tracer	✓	✗	✓	✗	✗	✓
Acquisition time	~ 1–2 min	~ 1.5–3 min	~ 5–10 min	~ 3–5 min	~ 5–10 min	~ 30–50 min
Signal-to-noise ratio	Low	Low	High	Low	Low	High
Parameters	CBV, CBF, MTT	ADC	k^{trans} , v_p , v_e , IAUC	CBF	Signal intensity (max, min, mean and range)	Tumour-to-brain uptake ratio (TBR)

Table 3. A comparison of each included method. * Based on computed subgroup averages.

to Kim and Shim's meta-analysis, which found an average sensitivity of 85% and specificity of 88% for detecting PsP using PET, since a later diagnosis predisposes to a more accurate one⁴⁰.

APT_w-MRI. APT_w-MRI was used to differentiate PsP and TTP in just one study. Ma and colleagues³¹ found APT_w-MRI to correctly identify 19 out of 20 patients in their TTP cohort (95%) and 11 out of 12 patients in their PsP cohort (92%). There was a marked signal increase in the TTP compared to PsP cohort, with an APT_wmean cut-off of 2.42% and an APT_wmax cut-off of 2.54%. This may be a promising method in the future, but further work on a larger dataset is required.

Combination methods. Multimodal approaches often demonstrate increased diagnostic accuracy and provide an additional layer of confidence compared to individual modalities. It is reasonable to assume the highest diagnostic accuracy would be achieved from the combination of results from already established modalities. However, the trade-off is the accompanied increase in cost and acquisition time. Regardless, with increasing availability of several above-mentioned modalities, the advantage of combination methods could be considered on a case-by-case basis.

Three combination methods were included in the present review. A combination of K^{trans} and rCBV maps obtained from DCE-MRI and DSC-MRI acquisitions, respectively, reported high sensitivity (88%) and specificity (91%) in a cohort of 98 patients²⁹. The maps could not discriminate between PsP and TTP in the cohort when used individually. Choi and colleagues²⁸ combined DSC-MRI with ASL and reported sensitivity and specificity of 94% and 82%, respectively, also finding the combination values higher than the individual methods. Lastly, Shi and colleagues²⁶ found that using DSC-MRI and DWI separately produced a specificity of 0.83 and 0.58, respectively. When used in combination, this increased to 92% overall. However, the combination also led to a decrease to 86% in sensitivity overall, despite DWI alone accurately identifying all 22 cases of tumour progression.

Clinical utility. Despite the large number of studies reporting the diagnostic potential of different imaging protocols, their routine clinical use has not been implemented. A summary of the main clinically relevant parameters is presented in Table 3^{41–43}.

An inherent limitation of using perfusion-weighted imaging is that while perfusion parameters are generally lower in PsP, the associated inflammatory response is likely to influence perfusion and lead to increased perfusion parameters such as rCBV⁴⁴. Similar effects have been seen with DWI as a result of radiation necrosis, suggesting decreased ADC may not always reflect a high cellularity and TTP⁴⁵. However, both PWI and DWI appear to demonstrate high overall diagnostic accuracy.

As the most commonly used perfusion MRI modality, DSC-MRI may be preferable for standard protocol due to its high clinical availability and short acquisition time that can be under one minute⁴³. The standardisation of rCBV discriminating cut-off values is limited by numerous potential imaging and data processing artifacts impeding accurate perfusion quantification as outlined by Willats and Calamante's 39 steps for accurate perfusion of DSC-MRI data⁴⁶. One of the most widely discussed issues is the possibility of contrast agent leakage into extracellular tissue, known as T1 shine-through effect⁴⁷. Application of model-based leakage corrections is advised for single-echo gadolinium-based DSC-MRI to account for the extent of vascular permeability⁴⁸.

DCE-MRI has a high signal-to-noise ratio compared to the other MR-perfusion techniques⁴⁹. The main limitation of this method is the relatively long data acquisition time, often over several minutes⁵⁰. Similar to other perfusion techniques, full quantification remains challenging due to difficulties with DCE tracer modelling. Efforts are currently undertaken to resolve issues related to accurate quantification of perfusion techniques. The establishment of taskforces such as the Quantitative Imaging Biomarkers alliance will facilitate clinical implementation of methods by providing reference measures and guidelines for best practices⁵¹.

ASL was a less frequently reported discriminating method compared to other perfusion methods. The main advantage of ASL over DSC-MRI is that it does not require a gadolinium-based bolus injection. It may therefore be more suitable for patients with contraindications to administration of contrast agents⁵². Furthermore, ASL can acquire entirely quantitative values of cerebral blood flow (CBF). A non-significant increase in sensitivity and specificity was observed when CBF measures acquired using ASL was combined with DSC-MRI, compared to use of the methods²⁸. Jovanovic and colleagues²⁷ concluded that the diagnostic accuracy of ASL was sufficient to replace DSC-MRI and therefore, avoid repeat follow-up contrast injections. An important consideration of

ASL is the longer acquisition time of 8–10 min at 1.5 T and 4–5 min at 3 T as well as significantly lower signal-to-noise ratio (SNR) compared to other perfusion methods⁴³.

APTw is a novel imaging technique demonstrated to detect the increased mobile protein content in brain tumours⁵³. Its full potential is yet to be established as U.S. Food and Drug Administration (FDA) approval of 3D-APTw for use on 3 T clinical MRI scanners was granted in 2018⁵⁴. However, APTw examinations may be time consuming (~ 5–10 min) and are susceptible to magnetic field inhomogeneities⁵⁵. Some work aims to optimise the signal-to-noise ratio and image acquisition speed⁵⁶. APTw is a promising method with initial studies reporting a high diagnostic accuracy, but larger datasets are needed to compare its performance against other techniques.

Despite the high reported sensitivity and specificity of 18F-FET PET, a long acquisition time of 50 min as reported by Galldiks and colleagues³⁰ limits clinical potential. Since 18F-FET PET relies on administration of labelled amino acid analogue, patients in the study were also required to fast for at least 12 h before scanning. In contrast to other radiotracers, the half-life of fluorine-18 is long enough to allow for off-site production. The requirement for pharmacokinetic analysis with compartment modelling⁵⁷ further limits potential for clinical implementation.

Future directions. Quantitative methods offer a more objective approach towards finding patterns in clinical data and enable more accurate diagnosis compared to qualitative methods^{58,59}. Jang and colleagues⁶⁰ recently applied a deep learning approach using convolutional neural networks to the differentiation of pseudoprogression and true progression and achieved a sensitivity of 87% and a specificity of 94.5%. Another study found a benefit of the combination of hypervascularity, cellularity and permeability parameters over single parameter measurements to distinguish the conditions⁶¹. The need for large datasets for training and testing radiomics models has led to a general lack of power, therefore future research should focus on increasing accessibility and data availability. National support for the scaling of technology and the potential use of artificial intelligence to aid clinical decision making has been outlined in the NHS Long Term Plan⁶².

Conclusion

Our systematic review and meta-analysis found DWI and DSC-MRI to have the highest diagnostic accuracy for differentiating between PsP and TTP. Considering the acquisition time and availability, DSC-MRI holds high potential for clinical implementation. The risk of repeat contrast agent injections required for DSC-MRI could be offset with the substitution of DSC-MRI for ASL. There was a clear advantage of using parameter cut-offs, over methods that relied on qualitative visual inspection. The diagnostic accuracy of methods such as PET, APTw-MRI, clinically feasible combination methods, and quantitative multiparametric techniques should be investigated in large-scale studies.

Received: 18 November 2021; Accepted: 14 July 2022

Published online: 02 August 2022

References

- Lapointe, S., Perry, A. & Butowski, N. A. Primary brain tumours in adults. *Lancet* **392**, 432–446. [https://doi.org/10.1016/S0140-6736\(18\)30990-5](https://doi.org/10.1016/S0140-6736(18)30990-5) (2018).
- Stupp, R. *et al.* Radiotherapy plus concomitant and adjuvant temozolomide for glioblastoma. *N. Engl. J. Med.* **352**, 987–996. https://doi.org/10.1056/NEJM043330/SUPPL_FILE/987SA1.PDF (2005).
- Fernandes, C. *et al.* Current Standards of Care in Glioblastoma Therapy. *Glioblastoma* **11**, 197–241 (2017).
- Birk, H. S., Han, S. J. & Butowski, N. A. Treatment options for recurrent high-grade gliomas. *CNS Oncol.* **6**, 61. <https://doi.org/10.2217/CNS-2016-0013> (2017).
- Thust, S. C., van den Bent, M. J. & Smits, M. Pseudoprogression of brain tumors. *J. Magn. Reson. Imaging* **48**, 571. <https://doi.org/10.1002/JMRI.26171> (2018).
- Ma, Y. M. *et al.* How to differentiate pseudoprogression from true progression in cancer patients treated with immunotherapy. *Am. J. Cancer Res.* **9**, 1546–1553 (2019).
- Reichert, A. & Jacobs, R. The impact of waiting time on patient outcomes: Evidence from early intervention in psychosis services in England. *Health Econ.* **27**, 1772. <https://doi.org/10.1002/HEC.3800> (2018).
- Abbasi, A. W. *et al.* Incidence of tumour progression and pseudoprogression in high-grade gliomas: A systematic review and meta-analysis. *Clin. Neuroradiol.* **28**, 401–411. <https://doi.org/10.1007/S00062-017-0584-X> (2018).
- Zikou, A. *et al.* Radiation necrosis, pseudoprogression, pseudoresponse, and tumor recurrence: Imaging challenges for the evaluation of treated gliomas. *Contrast Media Mol. Imaging* <https://doi.org/10.1155/2018/6828396> (2018).
- Brandma, D. *et al.* Clinical features, mechanisms, and management of pseudoprogression in malignant gliomas. *Lancet Oncol.* **9**, 453–461. [https://doi.org/10.1016/S1470-2045\(08\)70125-6](https://doi.org/10.1016/S1470-2045(08)70125-6) (2008).
- Fatterpekar, G. M. *et al.* Treatment-related change versus tumor recurrence in high-grade gliomas: A diagnostic conundrum—use of dynamic susceptibility contrast-enhanced (DSC) perfusion MRI. *AJR Am. J. Roentgenol.* **198**, 19–26. <https://doi.org/10.2214/AJR.11.7417> (2012).
- Ellingson, B. M. *et al.* Pseudoprogression, radionecrosis, inflammation or true tumor progression? challenges associated with glioblastoma response assessment in an evolving therapeutic landscape. *J. Neurooncol.* **134**, 495–504. <https://doi.org/10.1007/S11060-017-2375-2> (2017).
- Radbruch, A. *et al.* Pseudoprogression in patients with glioblastoma: Clinical relevance despite low incidence. *Neuro Oncol.* **17**, 151–159. <https://doi.org/10.1093/neuonc/nou129> (2015).
- Chukwueke, U. N. & Wen, P. Y. Use of the response assessment in neuro-oncology (RANO) criteria in clinical trials and clinical practice. *CNS Oncol.* **8**, 28. <https://doi.org/10.2217/CNS-2018-0007> (2019).
- Bramer, W. M., Rethlefsen, M. L., Kleijnen, J. & Franco, O. H. Optimal database combinations for literature searches in systematic reviews: A prospective exploratory study. *Syst. Rev.* **6**, 1–12. <https://doi.org/10.1186/S13643-017-0644-Y/TABLES/5> (2017).
- Moher, D. *et al.* Preferred reporting items for systematic review and meta-analysis protocols (PRISMA-P) 2015 statement. *Revista Espanola de Nutricion Humana y Dietetica* **20**, 148–160. <https://doi.org/10.1186/2046-4053-4-1/TABLES/4> (2016).
- Review Manager (RevMan) [Computer program]. Version 5.4, The Cochrane Collaboration (2020).

18. Stroup, D. F. *et al.* Meta-analysis of observational studies in epidemiology: A proposal for reporting. *J. Am. Med. Assoc.* **283**, 2008–2012. <https://doi.org/10.1001/jama.283.15.2008> (2000).
19. Whiting, P. F. *et al.* Quadas-2: A revised tool for the quality assessment of diagnostic accuracy studies. *Ann. Intern. Med.* **155**, 529–536 (2011).
20. Jones, C. M. & Athanasiou, T. Summary receiver operating characteristic curve analysis techniques in the evaluation of diagnostic tests. *Ann. Thorac. Surg.* **79**, 16–20. <https://doi.org/10.1016/J.ATHORACSUR.2004.09.040> (2005).
21. Higgins, J. P. T. & Thompson, S. G. Quantifying heterogeneity in a meta-analysis. *Stat. Med.* **21**, 1539–1558. <https://doi.org/10.1002/SIM.1186> (2002).
22. MIDAS: Stata module for meta-analytical integration of diagnostic test accuracy studies. <https://ideas.repec.org/c/boc/bocode/s456880.html>. Accessed 31 May 2022
23. Hozo, S. P., Djulbegovic, B. & Hozo, I. Estimating the mean and variance from the median, range, and the size of a sample. *BMC Med. Res. Methodol.* **5**, 1–10. <https://doi.org/10.1186/1471-2288-5-13/TABLES/3> (2005).
24. Kim, J. Y. *et al.* Incorporating diffusion- and perfusion-weighted MRI into a radiomics model improves diagnostic performance for pseudoprogression in glioblastoma patients. *Neuro Oncol.* **21**, 404. <https://doi.org/10.1093/NEUONC/NOY133> (2019).
25. Prager, A. J. *et al.* Diffusion and perfusion MRI to differentiate treatment-related changes including pseudoprogression from recurrent tumors in high-grade gliomas with histopathologic evidence. *AJNR Am. J. Neuroradiol.* **36**, 877. <https://doi.org/10.3174/AJNR.A4218> (2015).
26. Shi, W. *et al.* Diffusion kurtosis imaging combined with dynamic susceptibility contrast-enhanced MRI in differentiating high-grade glioma recurrence from pseudoprogression. *Eur. J. Radiol.* <https://doi.org/10.1016/J.EJRAD.2021.109941> (2021).
27. Jovanovic, M. *et al.* Differentiation between progression and pseudoprogression by arterial spin labeling MRI in patients with glioblastoma multiforme. *J. BUON* **22**, 1061–1067 (2017).
28. Choi, Y. J. *et al.* Pseudoprogression in patients with glioblastoma: Added value of arterial spin labeling to dynamic susceptibility contrast perfusion MR imaging. *Acta Radiol.* **54**, 448–454. <https://doi.org/10.1177/0284185112474916> (2013).
29. Elshafeey, N. *et al.* Multicenter study to demonstrate radiomic texture features derived from MR perfusion images of pseudoprogression compared to true progression in glioblastoma patients. *J. Clin. Oncol.* **35**, 1 (2017).
30. Galdiks, N. *et al.* Diagnosis of pseudoprogression in patients with glioblastoma using O-(2-[18F]fluoroethyl)-L-tyrosine PET. *Eur. J. Nucl. Med. Mol. Imaging* **42**, 685–695. <https://doi.org/10.1007/S00259-014-2959-4> (2015).
31. Ma, B. *et al.* Applying amide proton transfer-weighted MRI to distinguish pseudoprogression from true progression in malignant gliomas. *J. Magnet. Resonance Imaging* **44**, 456–462 (2016).
32. Young, R. J. *et al.* MRI perfusion in determining pseudoprogression in patients with glioblastoma. *Clin. Imaging* **37**, 41. <https://doi.org/10.1016/J.CLINIMAG.2012.02.016> (2013).
33. Sun, Y. Z. *et al.* Differentiation of pseudoprogression from true progression in glioblastoma patients after standard treatment: A machine learning strategy combined with radiomics features from T-1-weighted contrast-enhanced imaging. *BMC Med. Imaging* <https://doi.org/10.1186/s12880-020-00545-5> (2021).
34. Kerkhof, M. *et al.* Visual inspection of MR relative cerebral blood volume maps has limited value for distinguishing progression from pseudoprogression in glioblastoma multiforme patients. *CNS Oncol.* **6**, 297–306. <https://doi.org/10.2217/CNS-2017-0013> (2017).
35. von Hippel, P. T. The heterogeneity statistic I² can be biased in small meta-analyses. *BMC Med. Res. Methodol.* **15**, 1–8. <https://doi.org/10.1186/S12874-015-0024-Z/FIGURES/4> (2015).
36. Tsakiris, C. *et al.* Differentiation between true tumor progression of glioblastoma and pseudoprogression using diffusion-weighted imaging and perfusion-weighted imaging: Systematic review and meta-analysis. *World Neurosurg.* **144**, e100–e109. <https://doi.org/10.1016/J.WNEU.2020.07.218> (2020).
37. Martinez-Martinez, A. & Martinez-Bosch, J. Perfusion magnetic resonance imaging for high grade astrocytomas: Can cerebral blood volume, peak height, and percentage of signal intensity recovery distinguish between progression and pseudoprogression?. *Radiologia (Panama)* **56**, 35–43. <https://doi.org/10.1016/j.rx.2013.02.006> (2014).
38. Welker, K. *et al.* ASFN recommendations for clinical performance of MR dynamic susceptibility contrast perfusion imaging of the brain. *AJNR Am. J. Neuroradiol.* **36**, E41–E51. <https://doi.org/10.3174/AJNR.A4341> (2015).
39. Kebir, S. *et al.* A preliminary study on machine learning-based evaluation of static and dynamic FET-PET for the detection of pseudoprogression in patients with IDH-wildtype glioblastoma. *Cancers (Basel)* **12**, 1–14. <https://doi.org/10.3390/CANCERS1213080> (2020).
40. Kim, S. J. & Ryl Shim, S. Diagnostic value of radiolabeled amino acid PET for detection of pseudoprogression of brain tumor after treatment: a meta-analysis. *Nucl. Med. Commun.* **40**, 965–972. <https://doi.org/10.1097/MNM.0000000000001060> (2019).
41. Bammer, R. Basic principles of diffusion-weighted imaging. *Eur. J. Radiol.* **45**, 169–184. [https://doi.org/10.1016/S0720-048X\(02\)00303-0](https://doi.org/10.1016/S0720-048X(02)00303-0) (2003).
42. Jahng, G. H., Li, K. L., Ostergaard, L. & Calamante, F. Perfusion magnetic resonance imaging: A comprehensive update on principles and techniques. *Kor. J. Radiol.* **15**, 554–577. <https://doi.org/10.3348/KJR.2014.15.5.554> (2014).
43. Essig, M. *et al.* Perfusion MRI: The five most frequently asked technical questions. *AJR Am. J. Roentgenol.* **200**, 24–34. <https://doi.org/10.2214/AJR.12.9543> (2013).
44. Yoshii, Y. Pathological review of late cerebral radionecrosis. *Brain Tumor Pathol.* **25**, 51–58. <https://doi.org/10.1007/S10014-008-0233-9> (2008).
45. Asao, C. *et al.* Diffusion-weighted imaging of radiation-induced brain injury for differentiation from tumor recurrence. *AJNR Am. J. Neuroradiol.* **26**, 1455 (2005).
46. Willats, L. & Calamante, F. The 39 steps: evading error and deciphering the secrets for accurate dynamic susceptibility contrast MRI. *NMR Biomed.* **26**, 913–931. <https://doi.org/10.1002/NBM.2833> (2013).
47. Thompson, G. *et al.* Imaging biomarkers of angiogenesis and the microvascular environment in cerebral tumours. *Br. J. Radiol.* **84**, S127. <https://doi.org/10.1259/BJR/66316279> (2011).
48. Boxerman, J. L., Schmainda, K. M. & Weisskoff, R. M. Relative cerebral blood volume maps corrected for contrast agent extravasation significantly correlate with glioma tumor grade, whereas uncorrected maps do not. *AJNR: Am. J. Neuroradiol.* **27**, 859 (2006).
49. Dietrich, O., Biffar, A., Baur-Melnyk, A. & Reiser, M. F. Technical aspects of MR diffusion imaging of the body. *Eur. J. Radiol.* **76**, 314–322. <https://doi.org/10.1016/J.EJRAD.2010.02.018> (2010).
50. Chilla, G. S., Tan, C. H., Xu, C. & Poh, C. L. Diffusion weighted magnetic resonance imaging and its recent trend—a survey. *Quant. Imaging Med. Surg.* **5**, 407–422. <https://doi.org/10.3978/J.ISSN.2223-4292.2015.03.01> (2015).
51. McGehee, B. E., Pollock, J. M. & Maldjian, J. A. Brain perfusion imaging: How does it work and what should I use?. *J. Magn. Reson. Imaging* **36**, 1257–1272. <https://doi.org/10.1002/JMRI.23645> (2012).
52. Gulani, V. *et al.* Gadolinium deposition in the brain: Summary of evidence and recommendations. *Lancet Neurol* **16**, 564–570. [https://doi.org/10.1016/S1474-4422\(17\)30158-8](https://doi.org/10.1016/S1474-4422(17)30158-8) (2017).
53. Isobe, T. *et al.* Quantification of cerebral metabolites in glioma patients with proton MR spectroscopy using T2 relaxation time correction. *Magn Reson Imaging* **20**, 343–349. [https://doi.org/10.1016/S0730-725X\(02\)00500-3](https://doi.org/10.1016/S0730-725X(02)00500-3) (2002).
54. U.S. Food and Drug Administration (2018). https://www.accessdata.fda.gov/cdrh_docs/pdf17/K172920.pdf.
55. Zhou, J. *et al.* APT-weighted MRI: Techniques, current neuro applications, and challenging issues. *J. Magn. Reson. Imaging* **50**, 347–364. <https://doi.org/10.1002/JMRI.26645> (2019).

56. Zhou, J. Amide proton transfer imaging of the human brain. *Methods Mol. Biol.* **711**, 227–237. https://doi.org/10.1007/978-1-61737-992-5_10 (2011).
57. Debus, C. *et al.* Feasibility and robustness of dynamic 18F-FET PET based tracer kinetic models applied to patients with recurrent high-grade glioma prior to carbon ion irradiation. *Sci. Rep.* <https://doi.org/10.1038/s41598-018-33034-5> (2018).
58. Perry, L. A., Korfiatis, P., Agrawal, J. P. & Erickson, B. J. Increased signal intensity within glioblastoma resection cavities on fluid-attenuated inversion recovery imaging to detect early progressive disease in patients receiving radiotherapy with concomitant temozolomide therapy. *Neuroradiology* **60**, 35–42. <https://doi.org/10.1007/S00234-017-1941-9> (2018).
59. Sollmann, N. *et al.* Subtraction maps derived from longitudinal magnetic resonance imaging in patients with glioma facilitate early detection of tumor progression. *Cancers (Basel)* **12**, 1–14. <https://doi.org/10.3390/CANCERS12113111> (2020).
60. Jang, B. S. *et al.* Machine Learning Model to Predict Pseudoprogression versus Progression in Glioblastoma: A Multi-institutional Study (KROG 18–07). *Int. J. Radiat. Oncol. Biol. Phys.* **108**, 742. <https://doi.org/10.1016/j.ijrobp.2020.07.151> (2020).
61. Park, J. E. *et al.* Pseudoprogression in patients with glioblastoma: Assessment by using volume-weighted voxel-based multiparametric clustering of MR imaging data in an independent test set. *Radiology* **275**, 792–802. <https://doi.org/10.1148/radiol.14141414> (2015).
62. NHS. The NHS Long Term Plan. Published 2019. Accessed July 1, 2021. <https://www.longtermpplan.nhs.uk/wp-content/uploads/2019/01/nhs-long-term-plan-june-2019.pdf>.
63. Baek, H. J. *et al.* Percent change of perfusion skewness and kurtosis: A potential imaging biomarker for early treatment response in patients with newly diagnosed glioblastomas. *Radiology* **264**, 834–843. <https://doi.org/10.1148/RADIOL.12112120> (2012).
64. Cha, J. *et al.* Differentiation of tumor progression from pseudoprogression in patients with posttreatment glioblastoma using multiparametric histogram analysis. *AJNR Am. J. Neuroradiol.* **35**, 1309–1317. <https://doi.org/10.3174/AJNR.A3876> (2014).
65. Kong, D.-S. *et al.* Dynamic perfusion MR images can predict the pseudoprogression mimicking true progression in the treatment of newly diagnosed glioblastoma. *Neuro-Oncol.* **11**, 893. <https://doi.org/10.1215/15228517-2009-032> (2009).
66. Mangla, R. *et al.* Changes in relative cerebral blood volume 1 month after radiation-temozolomide therapy can help predict overall survival in patients with glioblastoma. *Radiology* **256**, 575–584. <https://doi.org/10.1148/RADIOL.10091440> (2010).
67. Mihailovic, J. & Dakovic, M. Advanced magnetic resonance techniques in early differentiation of pseudoprogression versus progression in the patients with glioblastoma multiforme. *Vojnosanit. Pregl.* **76**, 510–517. <https://doi.org/10.2298/VSP170114108M> (2019).
68. Bulik, M., Kazda, T., Slampa, P. & Jancalek, R. The diagnostic ability of follow-up imaging biomarkers after treatment of glioblastoma in the temozolomide era: Implications from proton MR spectroscopy and apparent diffusion coefficient mapping. *Biomed. Res. Int.* <https://doi.org/10.1155/2015/641023> (2015).
69. Chu, H. H. *et al.* Differentiation of true progression from pseudoprogression in glioblastoma treated with radiation therapy and concomitant temozolomide: Comparison study of standard and high-b-value diffusion-weighted imaging. *Radiology* **269**, 831–840. <https://doi.org/10.1148/radiol.13122024> (2013).
70. Kazda, T. *et al.* Advanced MRI increases the diagnostic accuracy of recurrent glioblastoma: Single institution thresholds and validation of MR spectroscopy and diffusion weighted MR imaging. *Neuroimage Clin.* **11**, 316–321. <https://doi.org/10.1016/j.nicl.2016.02.016> (2016).
71. Lee, W. J. *et al.* Diffusion-weighted MR imaging for the differentiation of true progression from pseudoprogression following concomitant radiotherapy with temozolomide in patients with newly diagnosed high-grade gliomas. *Acad Radiol.* **19**, 1353–1361. <https://doi.org/10.1016/j.acra.2012.06.011> (2012).
72. Patel, M. *et al.* Machine learning-based radiomic evaluation of treatment response prediction in glioblastoma. *Clin. Radiol.* **76**, 628. <https://doi.org/10.1016/j.crad.2021.03.019> (2021).
73. Reimer, C. *et al.* Differentiation of pseudoprogression and real progression in glioblastoma using ADC parametric response maps. *PLoS ONE* **12**, e0174620. <https://doi.org/10.1371/JOURNAL.PONE.0174620> (2017).
74. Song, Y. S. *et al.* True progression versus pseudoprogression in the treatment of glioblastomas: a comparison study of normalized cerebral blood volume and apparent diffusion coefficient by histogram analysis. *Kor. J. Radiol.* **14**, 662–672. <https://doi.org/10.3348/KJR.2013.14.4.662> (2013).
75. Feng, Wu. X. *et al.* Differentiating high-grade glioma recurrence from pseudoprogression: Comparing diffusion kurtosis imaging and diffusion tensor imaging. *Eur. J. Radiol.* <https://doi.org/10.1016/j.ejrad.2020.109445> (2021).
76. Yoo, R. E. *et al.* Independent poor prognostic factors for true progression after radiation therapy and concomitant temozolomide in patients with glioblastoma: Subependymal enhancement and low ADC value. *AJNR Am. J. Neuroradiol.* **36**, 1846–1852. <https://doi.org/10.3174/AJNR.A4401> (2015).
77. Nam, J. G. *et al.* Comparison between the prebolus T1 measurement and the fixed T1 value in dynamic contrast-enhanced MR imaging for the differentiation of true progression from pseudoprogression in glioblastoma treated with concurrent radiation therapy and temozolomide chemotherapy. *AJNR Am. J. Neuroradiol.* **38**, 2243–2250. <https://doi.org/10.3174/AJNR.A5417> (2017).
78. Suh, C. H. *et al.* Prediction of pseudoprogression in patients with glioblastomas using the initial and final area under the curves ratio derived from dynamic contrast-enhanced T1-weighted perfusion MR imaging. *AJNR Am. J. Neuroradiol.* **34**, 2278–2286. <https://doi.org/10.3174/AJNR.A3634> (2013).
79. Thomas, A. A. *et al.* Dynamic contrast enhanced T1 MRI perfusion differentiates pseudoprogression from recurrent glioblastoma. *J. Neurooncol.* **125**, 183–190. <https://doi.org/10.1007/S11060-015-1893-Z> (2015).
80. Yun, T. J. *et al.* Glioblastoma treated with concurrent radiation therapy and temozolomide chemotherapy: Differentiation of true progression from pseudoprogression with quantitative dynamic contrast-enhanced MR Imaging. *Radiology* **274**, 830–840. <https://doi.org/10.1148/radiol.14132632> (2014).
81. Sun, Y. Z. *et al.* Differentiation of pseudoprogression from true progression in glioblastoma patients after standard treatment: A machine learning strategy combined with radiomics features from T1-weighted contrast-enhanced imaging. *BMC Med. Imaging* <https://doi.org/10.1186/S12880-020-00545-5> (2021).

Acknowledgements

The authors would like to thank UCL Queen Square deputy librarian Kate Brunskill for support in devising the search strategy of the systematic review.

Author contributions

All authors contributed to the study conception and design. The literature search was performed by C.T., and data analysis was also performed by C.T., with assistance from J.O.E. and V.S. The first draft of the manuscript was written by C.T. and all authors commented on previous versions of the manuscript. Supervision and guidance were provided by G.S. and N.F. All authors read and approved the final manuscript.

Competing interests

The authors declare no competing interests.

Additional information

Supplementary Information The online version contains supplementary material available at <https://doi.org/10.1038/s41598-022-16726-x>.

Correspondence and requests for materials should be addressed to C.T.

Reprints and permissions information is available at www.nature.com/reprints.

Publisher's note Springer Nature remains neutral with regard to jurisdictional claims in published maps and institutional affiliations.



Open Access This article is licensed under a Creative Commons Attribution 4.0 International License, which permits use, sharing, adaptation, distribution and reproduction in any medium or format, as long as you give appropriate credit to the original author(s) and the source, provide a link to the Creative Commons licence, and indicate if changes were made. The images or other third party material in this article are included in the article's Creative Commons licence, unless indicated otherwise in a credit line to the material. If material is not included in the article's Creative Commons licence and your intended use is not permitted by statutory regulation or exceeds the permitted use, you will need to obtain permission directly from the copyright holder. To view a copy of this licence, visit <http://creativecommons.org/licenses/by/4.0/>.

© The Author(s) 2022